Phys. Status Solidi B **249,** No. 10, 1945–1950 (2012) / **DOI** 10.1002/pssb.201200356

Part of Special Issue
Phase-change memory: Science and applications

physica status solidi b
www.pss-b.com
basic solid state physics

Characterization of $Ge_2Sb_2Te_5$ thin film alloys using conductive-tip atomic force microscopy

Chia Min Chang[1,2], Yen Ju Liu[3], Ming Lun Tseng[3], Nien-Nan Chu[4], Ding-Wei Huang[1], Masud Mansuripur*[,5], and Din Ping Tsai[2,3,4,6]

[1] Graduate Institute of Photonics and Optoelectronics, National Taiwan University, Taipei, Taiwan
[2] Department of Physics, National Taiwan University, Taipei, Taiwan
[3] Graduate Institute of Applied Physics, National Taiwan University, Taipei, Taiwan
[4] Instrument Technology Research Center, National Applied Research Laboratories, Hsinchu, Taiwan
[5] College of Optical Sciences, The University of Arizona, Tucson, Arizona, USA
[6] Research Center for Applied Sciences, Academia Sinica, Taipei, Taiwan

Received 12 June 2012, revised 21 June 2012, accepted 30 July 2012
Published online 24 August 2012

Dedicated to Stanford R. Ovshinsky on the occasion of his 90th birthday

Keywords electronic data storage, materials and process characterization, optical recording, phase-change materials

* Corresponding author: e-mail masud@optics.arizona.edu, Phone: +520-621-4879, Fax: +520-621-4385,
Web: www.optics.arizona.edu/masud/

Conductive-tip atomic force microscopy (C-AFM) is a powerful tool for investigating the electrical characteristics of phase-change materials commonly used for electronic and optical data storage. We demonstrate the usefulness of this technique by examining the electrical conductivity of crystalline marks recorded with a focused laser pulse on a thin $Ge_2Sb_2Te_5$ film.

1 Introduction Stanford Ovshinsky pioneered the field of disordered materials that can be reversibly changed between amorphous and crystalline states by an energy source, such as electricity or a laser beam [1–3]. His discovery of amorphous chalcogenides has revolutionized the fields of electronic and optical data storage [4–16]. This paper, which is dedicated to "Stan," as his friends and admirers call him, briefly explores certain properties of thin films of $Ge_2Sb_2Te_5$, a leading candidate for both reversible electrical and erasable optical memories.

Figure 1(a) shows the stack structure used in our experiments. Here a glass substrate is first coated with 130 nm of ZnS–SiO_2 dielectric layer, then covered with a 5 nm-thick gold film that acts as the bottom electrode in our Conductive-tip atomic force microscopy (C-AFM) measurements (MFP-3D^{TM}, Asylum Research). A 10 nm-thick amorphous $Ge_2Sb_2Te_5$ layer (GST) is finally deposited over the gold layer. The deposition is done in a conventional magnetron sputtering system, and the recording of lines and marks on the GST sample is carried out using a static test-bed in which pulses from a $\lambda = 658$ nm semiconductor laser are focused on the sample surface via a 0.65 NA diffraction-limited objective lens.

Our C-AFM cantilever probe is coated with $PtIr_5$ and is connected to the virtual ground, as shown in Fig. 1(a). An SEM image of the C-AFM tip is shown in Fig. 1(b). The bias voltage V_{bias} is applied to the gold film through the application of silver paste and conductive carbon tape to a region of the sample that is about 10 mm away from the area on which various laser-written marks are located.

In what follows, we present optical, AFM, and C-AFM images of laser-recorded marks on amorphous GST films. We find that our C-AFM image contrast is significantly enhanced when parallel straight lines are carved into the sample by laser ablation, straight lines that define amorphous GST stripes with an approximate width of 5–10 μm. Additional information and further detail can be found in our previous publications on the subject [17–25].

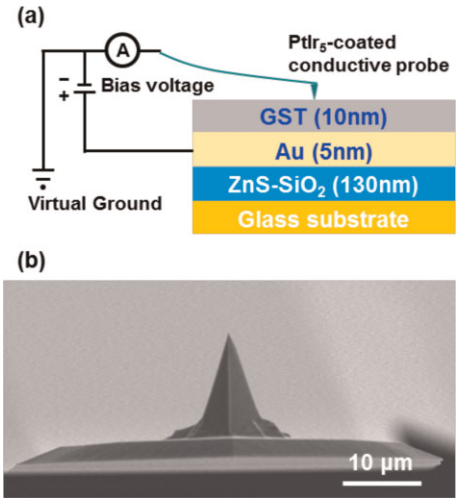

Figure 1 (online colour at: www.pss-b.com) (a) Diagram of the experimental setup, depicting a conductive-tip AFM monitoring the local electrical resistivity of a sputter-deposited ZnS–SiO_2(130 nm)/Au(5 nm)/$Ge_2Sb_2Te_5$(10 nm) stack atop a glass substrate. (b) SEM image of the conductive probe, which is coated with a thin layer of $PtIr_5$.

2 Recording parallel straight lines When writing straight lines on the GST film using a focused continuous-wave (CW) laser beam, we have control over the laser power P_o and the stage velocity V_o. Figure 2 shows the results of writing five pairs of straight lines at $V_o = 100\,\mu m\,s^{-1}$ using different laser powers, starting with $P_o = 2\,mW$ on the right-hand side, and increasing the power in increments of 0.5 mW up to $P_o = 4\,mW$ on the left-hand side. With the increasing laser power up to about 2.5 mW, the recorded lines become more and more conductive, but ablation sets in at $P_o \approx 3\,mW$. The line-pair on the right-hand side of Fig. 2(b) is probably crystalline, as it shows a change in the density/thickness of the film, but crystallization has not yet led to a pronounced change in conductivity [26]. The conductivity of individual crystalline grains does not seem to depend strongly on the laser power. The regions in between the recorded lines, whether these lines are crystalline or ablated, remain amorphous. Neither the AFM nor the C-AFM image in Fig. 2(b,c) indicate any changes in the topology or the conductivity of the amorphous stripes located between adjacent lines.

The results of recording straight lines on the GST sample with a fixed laser power at different stage velocities are shown in Fig. 3. The three line-pairs in this figure were recorded at $P_o = 2.8\,mW$ and $V_o = 50$, 75, and $100\,\mu m\,s^{-1}$, respectively. At the slow scanning rate of $V_o = 50\,\mu m\,s^{-1}$, ablation appears to be setting in. This is not visible in the optical image of Fig. 3(a), but inferred from the AFM image in Fig. 3(b). Frames (d, e) of Fig. 3 are magnified views of the line-pair appearing on the left-hand side of the frames (a–c), clearly indicating the onset of ablation. Apparently, the nonuniform stage motion consists of a series of discontinuous jumps. In all cases, crystallization of the lines does not

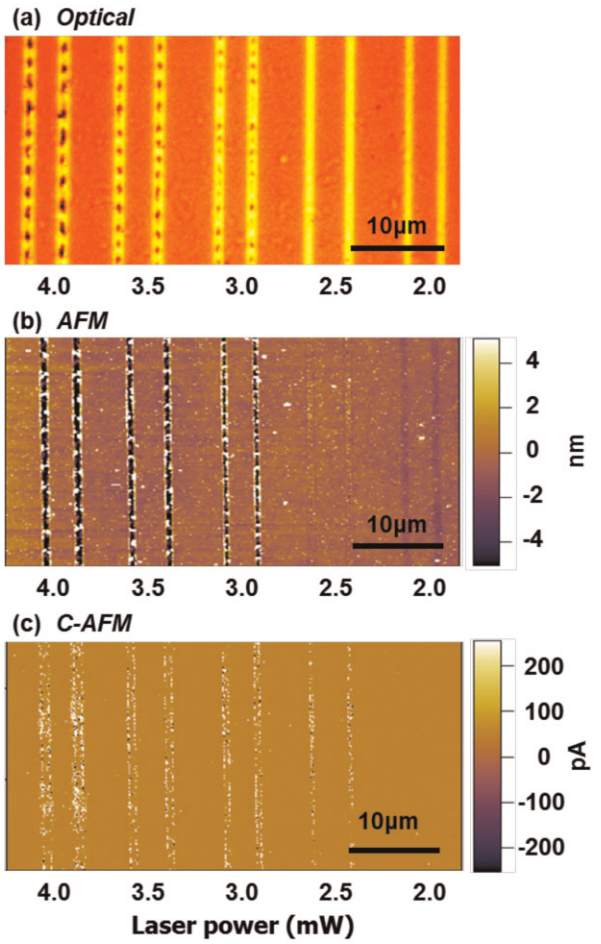

Figure 2 (online colour at: www.pss-b.com) (a) Optical microscope image of pairs of parallel straight lines recorded on the stack of Fig. 1(a) at different laser powers (2–4 mW) under the fixed stage velocity of $100\,\mu m\,s^{-1}$. While the as-deposited GST film remains amorphous, the recorded lines are either crystalline or ablated. (b) AFM and (c) C-AFM images of the same region of the sample. The C-AFM image was acquired with $V_{bias} = 50\,mV$ at a current gain of $2\,nA\,V^{-1}$.

seem to affect/modify the amorphous stripes in between adjacent line-pairs. At high magnification, however, weakly conducting spots appear to be present at random in the amorphous regions; see Fig. 3(e).

We mention in passing that the scale-bars used for AFM and C-AFM images are generally chosen for the highest possible image contrast, which requires striking the right balance between the signal and noise levels.

3 Characterization of marks recorded on amorphous GST stripes Figure 4 shows optical, AFM, and C-AFM images of a series of marks recorded with different laser powers (4–20 mW) and pulse durations (100–1500 ns) on the amorphous stripes that are defined by an array of crystalline lines. The lines themselves were recorded with a focused CW laser beam at $P_o = 2.5\,mW$ and with a

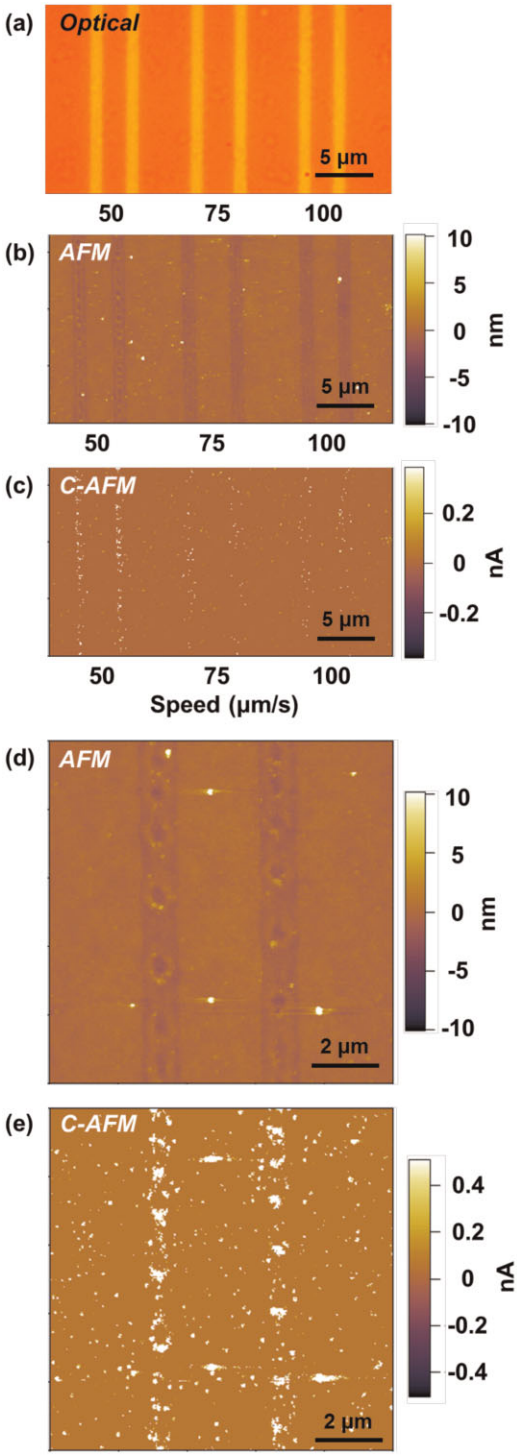

Figure 3 (online colour at: www.pss-b.com) (a) Reflection optical microscope image of straight line pairs recorded on the stack of Fig. 1(a) with a fixed laser power of 2.8 mW at different stage velocities of 50, 75, and 100 $\mu m\,s^{-1}$. (b) AFM and (c) C-AFM images of the same region of the sample. (d, e) Magnified AFM and C-AFM images, respectively, of the line pair recorded at $V_o = 50\,\mu m\,s^{-1}$. The C-AFM images in (c) and (e) were acquired with $V_{bias} = 100$ mV and a current gain of 2 nA V^{-1}.

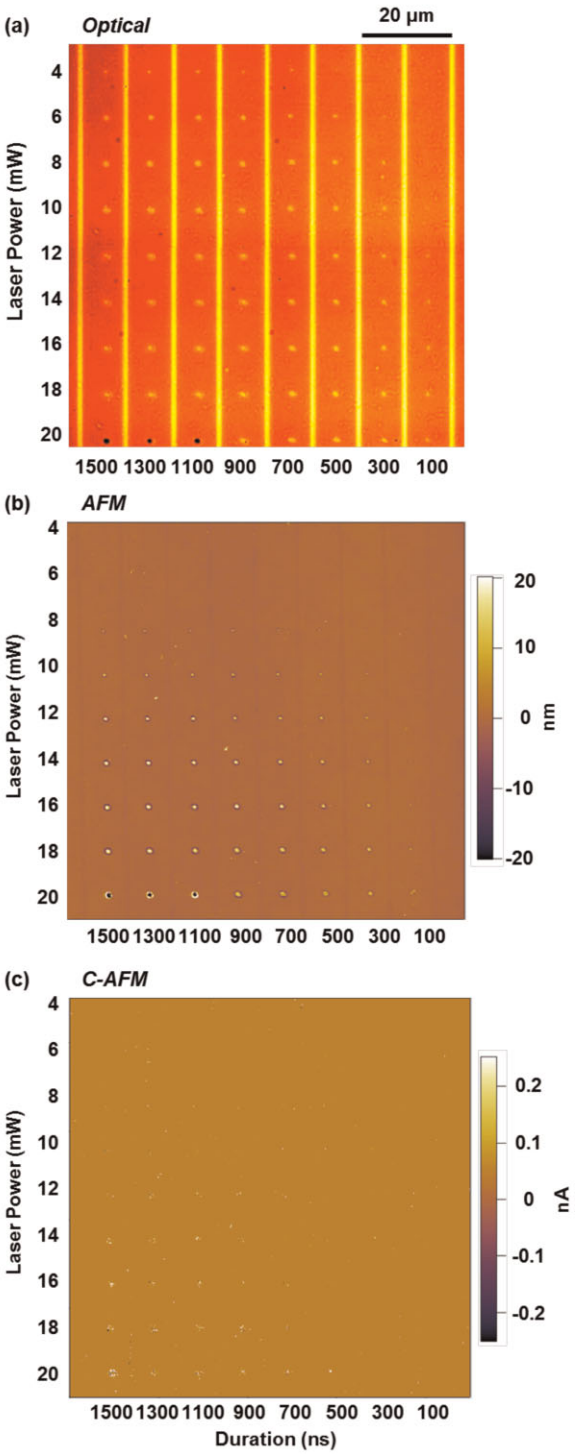

Figure 4 (online colour at: www.pss-b.com) (a) Reflection optical microscope image of marks recorded with different laser powers (4–20 mW) and pulse durations (100–1500 ns) on the stack structure depicted in Fig. 1(a). Also written on this sample are straight crystalline lines with a focused CW laser beam at $P_o = 2.5$ mW and a stage velocity $V_o = 100\,\mu m\,s^{-1}$. (b) AFM and (c) C-AFM images of recorded marks and crystalline lines in the same region of the sample. The C-AFM image in (c) was acquired with $V_{bias} = 50$ mV and a current gain of 2 nA V^{-1}.

stage velocity of $V_o = 100\,\mu m\,s^{-1}$. In the C-AFM image of Fig. 4(c) the crystalline lines are barely visible, indicating that the degree and/or depth of crystallization has been insufficient to create a conductive path to the gold under-layer. Note that our general procedure for presenting AFM and C-AFM images is to choose the corresponding scale-bars for maximum image contrast. Thus the fact that the C-AFM image in Fig. 4(c) fails to reveal the existence of many of the smaller marks is an indication that the small-mark signals in this instance are below the noise level.

In Fig. 5 we show images of the same set of recorded marks as in Fig. 4, but the straight lines in this case were written with a 10 mW focused laser beam at a speed of $100\,\mu m\,s^{-1}$. The highly crystallized boundaries of the ablated lines are electrically conductive, forming a continuous path from the various regions of the sample to the grounding pad, which is pasted on the lower part of the sample (not shown). The recorded marks in Fig. 5(c) exhibit higher C-AFM image contrast relative to those in Fig. 4(c), presumably because the crystalline lines in Fig. 4, unlike the ablated lines in Fig. 5, have failed to make proper contact with the gold under-layer. Another difference between the two cases is that, in the case of Fig. 4, the gold under-layer has remained intact, whereas in Fig. 5 the high-power laser beam has carved a groove into the gold layer as well, making the GST stripes electrically disconnected from the adjacent stripes. Whether or not this electrical isolation of the amorphous stripes plays a role in the improved C-AFM image contrast is not clear at this point.

Figure 6 shows AFM and C-AFM images of two of the marks recorded within the stripe regions in between the ablated lines of Fig. 5. The mark depicted in (a,b) is written with an 18 mW–100 ns laser pulse, and appears in the AFM image to be depressed at the boundary but slightly bulging at the center. The nature of electrical conductivity in the bulge region is spotty, either as a result of partial crystallization within the melt-quenched amorphous bulge, or because of a slight detachment of the GST film from the gold under-layer; see Fig. 6(b). In contrast, the mark depicted in Fig. 6(c,d), written with a 6 mW–500 ns laser pulse, has a central disk that appears in the C-AFM image to be fully crystallized, as it exhibits a solid conductive patch surrounded by a slightly depressed, amorphous ring. Note that the cross-sectional profiles shown below each frame of Fig. 6 are plotted over the full range of 0–20 nA.

In Fig. 7, we compare the current–voltage (I–V) curves obtained from the central regions of two different marks, one written with a 6 mW–300 ns laser pulse and shown in frame (a), the other written with a 4 mW–1100 ns laser pulse and shown in frame (b). The I–V curve of the mark in Fig. 7(a) clearly shows amorphous behavior (i.e., low electrical conductivity), with the current ranging in the ± 1.5 nA interval when the bias voltage is scanned in the ± 300 mV range. The AFM image of the mark, shown in the inset, is reminiscent of the bulged mark depicted in Fig. 6(a). In Fig. 7(b), the I–V curve indicates excellent crystalline behavior (i.e., high electrical conductivity), with the current

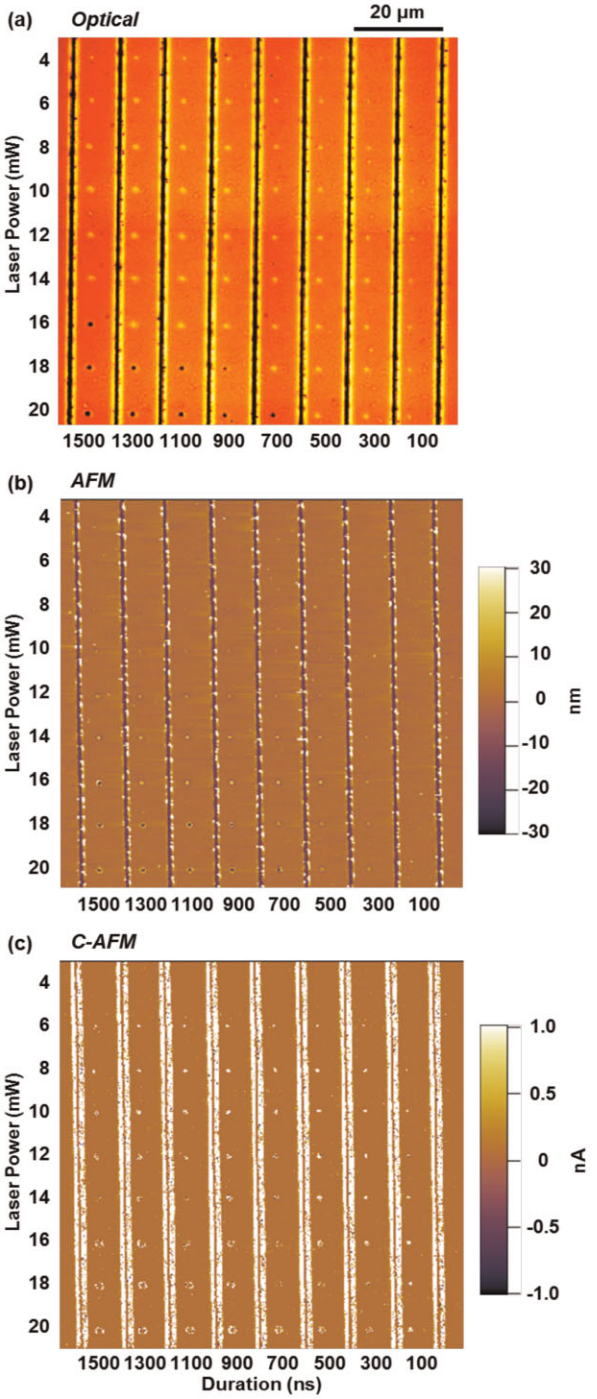

Figure 5 (online colour at: www.pss-b.com) (a) Reflection optical microscope image of marks recorded with different laser powers (4–20 mW) and pulse durations (100–1500 ns) on the stack structure of Fig. 1(a). Also written on this sample are ablated straight lines with a CW laser power of $P_o = 10$ mW at a velocity of $V_o = 100\,\mu m\,s^{-1}$. (b) AFM and (c) C-AFM images of recorded marks and ablated lines in the same region of the sample. The C-AFM image in (c) is acquired with a bias voltage of 50 mV and a current gain of $2\,nA\,V^{-1}$.

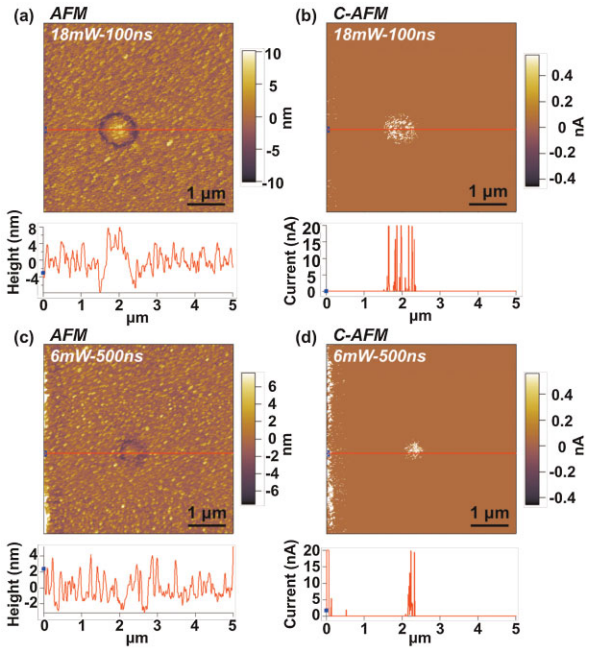

Figure 6 (online colour at: www.pss-b.com) (a, b) AFM and C-AFM images (including cross-sectional profiles) of a mark recorded by an 18 mW–100 ns laser pulse on the GST film with ablated lines depicted in Fig. 5. The C-AFM image in (b) was acquired with $V_{bias} = 50$ mV, where the full range of the current signal was 0–20 nA. (c, d) Images of a mark recorded by a 6 mW–500 ns laser pulse under otherwise identical circumstances.

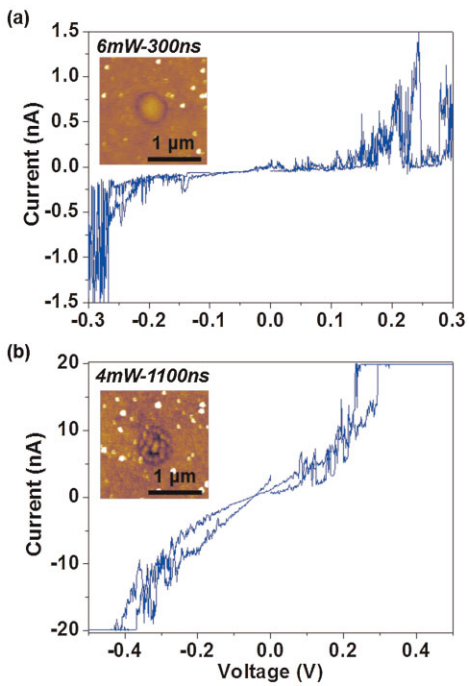

Figure 7 (online colour at: www.pss-b.com) Current–voltage (*I–V*) curves obtained at the center of two marks recorded on the GST film in between the ablated lines depicted in Fig. 5. The laser pulse used to record the mark was (a) 6 mW–300 ns and (b) 4 mW–1100 ns. AFM images of the marks appear in the insets.

varying between ±20 nA when the bias voltage is scanned in the range of ±400 mV. The AFM image of the mark in this case, again shown in the inset, is reminiscent of the well-crystallized mark depicted in Fig. 6(b). Note that the nonlinear character of the *I–V* curve in Fig. 7(b) is *not* an indication of electric breakdown in the resistivity of the spot under consideration, since the curve retraces itself upon reversing the voltage.

Finally, Fig. 8 shows the results of repeated C-AFM measurements of the same mark that has been recorded with a 6 mW–300 ns laser pulse within an amorphous stripe defined by a pair of ablated lines; see Fig. 8(a) for an AFM image of the mark and its immediate surroundings. The three scans of the same region shown in frames (b)–(d) at $V_{bias} = 50$ mV show a fading of the contrast, presumably due to a deterioration of the C-AFM probe tip, which is working in the contact mode, or perhaps because the properties of the GST material are changing as a result of contact with the C-AFM tip. Frames (e)–(g) of Fig. 8 show a second set of three scans of the same region, with bias voltages of 100, 150, and 200 mV, respectively. The image contrast remains apparently unchanged in these three frames,

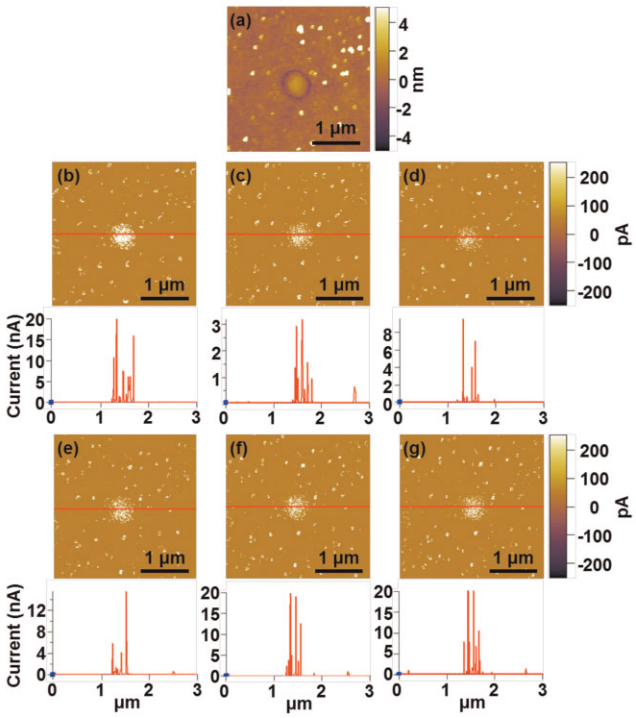

Figure 8 (online colour at: www.pss-b.com) Calibration process of C-AFM. Images of a mark recorded with a 6 mW–300 ns laser pulse on the GST film with the ablated lines depicted in Fig. 5. Each C-AFM image is accompanied by the corresponding cross-sectional profile. (a) AFM image of the recorded mark and its surroundings. (b–d) Repeated C-AFM images of the same spot, acquired with the same bias voltage of 50 mV and current gain of 2 nA V^{-1}. (e–g) C-AFM images of the same region of the sample, obtained with $V_{bias} = 100$, 150, and 200 mV, respectively.

indicating that perhaps the increased bias is canceling the effects of tip/sample deterioration.

The cross-sectional profiles in Fig. 8 vary significantly in shape and in magnitude from one scan to the next. This is not surprising, however, considering that a slight mis-registration of the scan coordinates can result in such variations. What is remarkable here is the discrete nature of the crystallinity of recorded marks, which is consistently observed in all our C-AFM measurements.

4 Concluding remarks We have shown that C-AFM is a powerful tool for studies of phase-change materials used in both electronic and optical memories. In many instances, when a recorded mark is too small to be recognized by optical or atomic force microscopy, the C-AFM scans not only reveal the existence as well as the shape and location of the mark, but also enable direct measurements of the *I*–*V* curves on nanometer-sized regions within and at the boundaries of the mark. The C-AFM signal contrast can be enhanced if crystalline marks are recorded within amorphous stripes defined by ablated lines carved into both the GST film and the conductive underlayer, which underlayer acts as an electrode in C-AFM measurements. The spotty nature of the conductivity maps of various laser-written marks clearly indicates the formation of thin conductive filaments through the thickness of the GST film.

Acknowledgements The authors acknowledge financial support from National Science Council, Taiwan, under grant numbers 99-2120-M-002-012, 99-2911-I-002-127, 100-2120-M-002-008, and 100-2923-M-002-007-MY3. We are also grateful to National Center for Theoretical Sciences, Taipei Office, Molecular Imaging Center of National Taiwan University, and Research Center for Applied Sciences, Academia Sinica, Taiwan, for their support.

References

[1] S. R. Ovshinsky, Phys. Rev. Lett. **21**, 1450–1453 (1968).
[2] S. R. Ovshinsky, Disordered Materials: Science, Technology: Selected Papers (Amorphous Institute Press, Bloomfield Hills, MI, 1982).
[3] H. Fritzsche and B. Schwartz, The Science and Technology of an American Genius: Stanford R. Ovshinsky (World Scientific, Singapore, 2008).
[4] M. Wuttig and N. Yamada, Nature Mater. **6**, 824–832 (2007).
[5] M. Wuttig and C. Steimer, Appl. Phys. A **87**, 411–417 (2007).
[6] Y. Jung, S.-W. Nam, and R. Agarwal, Nano Lett. **11**, 1364–1368 (2011).
[7] D. Krebs, S. Raoux, C. T. Rettner, G. W. Burr, R. M. Shelby, M. Salinga, C. M. Jefferson, and M. Wuttig, J. Appl. Phys. **106**, 054308 (2009).
[8] N. Yamada, E. Ohno, K. Nishiuchi, N. Akahira, and M. Takao, J. Appl. Phys. **69**, 2849 (1991).
[9] I. Friedrich, V. Weidenhof, S. Lenk, and M. Wuttig, Thin Solid Films **389**, 239–244 (2001).
[10] M. Chen, K. A. Rubin, and R. W. Barton, Appl. Phys. Lett. **49**, 502–504 (1986).
[11] N. Yamada and T. Matsunaga, J. Appl. Phys. **88**, 7020–7028 (2000).
[12] J. Kalb, F. Spaepen, and M. Wuttig, Appl. Phys. Lett. **84**, 5240–5242 (2004).
[13] J. H. Coombs, A. P. J. M. Jongenelis, W. Vanesspiekman, and B. A. Jacobs, J. Appl. Phys. **78**, 4918–4928 (1995).
[14] C. Peng, L. Cheng, and M. Mansuripur, J. Appl. Phys. **82**, 4183–4191 (1997).
[15] M. Mansuripur, J. K. Erwin, W. Bletscher, P. Khulbe, K. Sadeghi, X. Xun, A. Gupta, and S. Mendes, Appl. Opt. **38**, 7095–7104 (1999).
[16] P. Khulbe, E. M. Wright, and M. Mansuripur, J. Appl. Phys. **88**, 3926–3933 (2000).
[17] S. K. Lin, P. L. Yang, I. C. Lin, H. W. Hsu, and D. P. Tsai, Jpn. J. Appl. Phys. **45**(2B), 1431–1434 (2006).
[18] S. K. Lin, I. C. Lin, and D. P. Tsai, Opt. Express **14**, 4452–4458 (2006).
[19] S.-H. Chen, S.-P. Hou, J. H. Hsieh, H. K. Chen, and D. P. Tsai, J. Vac. Sci. Technol. A **24**, 2003–2007 (2006).
[20] S. K. Lin, I. C. Lin, S. Y. Chen, H. W. Hsu, and D. P. Tsai, IEEE Trans. Magn. **43**, 861–863 (2007).
[21] C. H. Chu, B. J. Wu, T. S. Kao, Y. H. Fu, H. P. Chiang, and D. P. Tsai, IEEE Trans. Magn. **45**, 2221–2223 (2009).
[22] C. H. Chu, C. D. Shiue, H. W. Cheng, M. L. Tseng, H. P. Chiang, M. Mansuripur, and D. P. Tsai, Opt. Express **18**, 18383–18393 (2010).
[23] C. M. Chang, C. H. Chu, M. L. Tseng, H. P. Chiang, M. Mansuripur, and D. P. Tsai, Opt. Express **19**, 9492–9504 (2011).
[24] C. H. Chu, M. L. Tseng, C. D. Shiue, S. W. Chen, H. P. Chiang, M. Mansuripur, and D. P. Tsai, Opt. Express **19**, 12652–12657 (2011).
[25] M. L. Tseng, B. H. Chen, C. H. Chu, C. M. Chang, W. C. Lin, N. N. Chu, M. Mansuripur, A. Q. Liu, and D. P. Tsai, Opt. Express **19**, 16975–16984 (2011).
[26] T. Siegrist, P. Jost, H. Volker, M. Woda, P. Merkelbach, C. Schlockermann, and M. Wuttig, Nature Mater. **10**, 202–208 (2011).

